Pseudobinary approach to the discovery and design of copper-based sulfides

Takashi Hagiwara, Koichiro Suekuni, Pierric Lemoine, Carmelo Prestipino, Erik Elkaim, Andrew R. Supka, Rabih Al Rahal Al Orabi, Marco Fornari, Emmanuel Guilmeau, Bernard Raveau, et al.

A Pseudo-Binary Approach to the Discovery and Design of Copper-based Sulphides

Takashi Hagiwara,[1] Koichiro Suekuni,[1,2*] Pierric Lemoine,[3,4*†] Carmelo Prestipino,[3] Erik Elkaim,[5] Andrew R. Supka,[6] Rabih Al Rahal Al Orabi,[6] Marco Fornari,[6*] Emmanuel Guilmeau,[7*] Bernard Raveau,[7] Hikaru Saito,[8] Philipp Sauerschnig,[9] Michihiro Ohta,[9] Yui Kanemori,[10] and Michitaka Ohtaki[1,2]

1 Department of Applied Science for Electronics and Materials, Interdisciplinary Graduate School of Engineering Sciences, Kyushu University, Kasuga, Fukuoka 816–8580, Japan

2 Transdisciplinary Research and Education Center for Green Technologies, Kyushu University, Kasuga, Fukuoka 816-8580, Japan

3 Université de Rennes 1, CNRS, ISCR-UMR 6226, F-35000 Rennes, France

4 Institut Jean Lamour, UMR7198 CNRS, Université de Lorraine, 54011 Nancy, France

5 Synchrotron Soleil, Saint-Aubin, BP 48, 91192 Gif-sur-Yvette, France

6 Department of Physics and Science of Advanced Materials Program, Central Michigan University, Mt. Pleasant, Michigan 48859, USA

7 CRISMAT, CNRS, Normandie Université, ENSICAEN, UNICAEN, 14000 Caen, France

8 Institute for Materials Chemistry and Engineering, Kyushu University, Kasuga, Fukuoka 816-8580, Japan

9 Global Zero Emission Research Center, National Institute of Advanced Industrial Science and Technology (AIST), Tsukuba, Ibaraki 305-8569, Japan

10 Department of Energy Science and Engineering, Faculty of Engineering, Kyushu University, Motooka, Fukuoka 819-0395, Japan

ABSTRACT: Copper-based sulphide semiconductors with structure based on a sphalerite-like network can provide environmentally sound solutions to thermoelectric and photovoltaic energy conversion at low cost. In this study, we report the synthesis and characterization of a copper-based sulphide, $Cu_{30}Ti_6Sb_2S_{32}$, discovered within the pseudo-binary Cu_3SbS_4–Cu_4TiS_4 system. This new compound crystallizes in a colusite-like cubic structure, which is characterized by "interstitial" Ti atoms forming tetrahedral-octahedral $[TiS_4]Cu_6$ complexes linearly arranged within the Cu-S corner-sharing matrix. The $[TiS_4]Cu_6$ units arrangement distinguishes the crystal structures of $Cu_{26}Ti_2Sb_6S_{32}$ (isolated units, 0D linkage), $Cu_{30}Ti_6Sb_2S_{32}$ (chain of linked units, 1D), and Cu_4TiS_4 (plane of linked units, 2D). We emphasize the semiconducting nature and the low thermal conductivity. The electronic structure and the vibrational properties are investigated by the combination of experiments and first-principles calculations. We demonstrate that a design approach based on the pseudo-binary composition, here with the generic formula $(Cu_3SbS_4)_{1-x}(Cu_4TiS_4)_x$, is a fruitful direction for the discovery of new copper-based sulphides with tunable transport properties.

INTRODUCTION

Complex copper-based sulphides have been the subject of numerous investigations, in particular for thermoelectric and photovoltaic applications (for a review see Ref. 1). Many thermoelectric (TE) copper-based sulphides[2–11,12–19,20–27,28–34,35–39] have been explored and, besides tetrahedrites, colusites $Cu_{26}T_2M_6S_{32}$ (T = Ti, V, Nb, Ta, Cr, Mo, W; M = Sn, Ge, Sb) stand out by their performances that approach a thermoelectric figure of merit, *ZT*, of 1 around 700 K. In the colusite structure, a critical component responsible for the TE performance is the sphalerite-like (*i.e.* zincblende-like) network (Figure 1). Interestingly, high photovoltaic conversion efficiency is also obtained for sphalerite derivatives, *e.g.* Cu–Sn–S compounds, chalcopyrite derivative $Cu(In,Ga)S_2$, and kesterite Cu_2ZnSnS_4.[40,41] Extensive research on both thermoelectric and photovoltaic materials suggests that sulphides involving a copper-rich sphalerite-like $Cu_{1-x}M_xS$ framework should be regarded as promising candidates for energy conversion technologies.

In the sphalerite-derivative compounds, the majority element, monovalent copper, forms a three-dimensional Cu–S network built up of corner-sharing CuS_4 tetrahedra; indeed, the valence band is mainly composed of hybridized electronic orbitals of Cu and S. Doping the M sites of the $Cu_{1-x}M_xS$ network may induce *p*-type electronic conductivity due the possibility of charge delocalization associated with Cu^{2+}/Cu^{+} oxidation.[42] This is exemplified by the boosting of thermoelectric performance of the famatinite

Cu_3SbS_4 (an ordered sphalerite-derivative phase; Figure 1) by doping the Sb^{5+} sites with Ge^{4+} cations.[12]

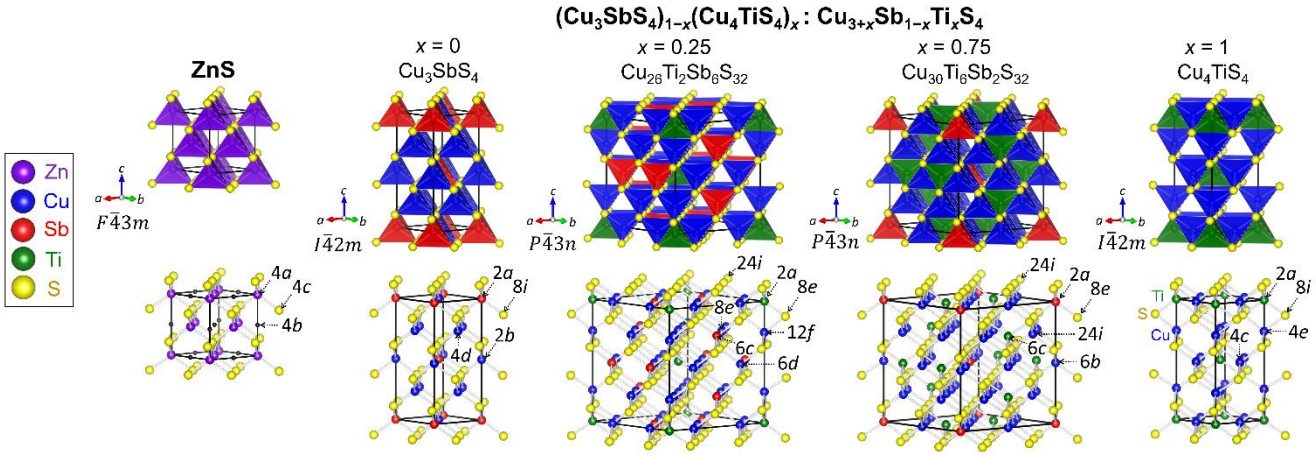

Figure 1. Crystal structure representations of sphalerite (ZnS) and the phases encountered in the pseudo-binary system $(Cu_3SbS_4)_{1-x}(Cu_4TiS_4)_x$, *i.e.*, $Cu_{3+x}Sb_{1-x}Ti_xS_4$: Cu_3SbS_4 (x = 0), $Cu_{26}Ti_2Sb_6S_{32}$ (x = 0.25, colusite), $Cu_{30}Ti_6Sb_2S_{32}$ (x = 0.75), and Cu_4TiS_4 (x = 1). For the representation of sphalerite, the 4*a* site is occupied by Zn atoms, while the 4*b* site is empty.

An important feature of the sphalerite-like $Cu_{1-x}M_xS$ network involves the presence of interstitial tetrahedral sites that can be partially occupied by d^0 cations, *e.g.*, Ti^{4+}, V^{5+}, and Cr^{6+} as in colusite phases.[28–34,35–39] An example of colusite is $Cu_{26}Ti_2Sb_6S_{32}$, which exhibits semiconducting properties and low thermal conductivity, κ.[38] Similar to Cu_3SbS_4, the electrical resistivity, ρ, of this phase decreases by the substitution of Ge^{4+} for Sb^{5+} (hole doping), leading to high thermoelectric performance. The colusite $Cu_{26}Ti_2Sb_6S_{32}$ crystallizes in a cubic structure with space group $P\bar{4}3n$, where CuS_4 and SbS_4 tetrahedra share their corners forming a $Cu_{26}Sb_6S_{32}$ sphalerite host lattice whose tetrahedral interstitial sites are occupied in an ordered fashion by two d^0 Ti^{4+} cations per formula unit (*i.e.* two per unit cell) (Figure 1). The higher Ti content on the tetrahedral interstitial sites is shown by the Cu_4TiS_4 sulphide[43] (Figure 1), whose sphalerite network Cu_4S_4 accommodates one d^0 Ti^{4+} cation per formula unit (*i.e.* two per unit cell). It should be noted that the crystal structure of $Cu_{26}Ti_2Sb_6S_{32}$ colusite is characterized by combined features of Cu_3SbS_4 (Cu/Sb–S sphalerite host) and Cu_4TiS_4 (Cu–S sphalerite host and interstitial Ti). Furthermore, the composition of $Cu_{26}Ti_2Sb_6S_{32}$ can be described as $(Cu_3SbS_4)_{1-x}(Cu_4TiS_4)_x$ with x = 0.25.

The important structural role of the sphalerite matrix in the pseudo-binary Cu_3SbS_4–Cu_4TiS_4 system suggests that other phases with the generic formulation $(Cu_3SbS_4)_{1-x}(Cu_4TiS_4)_x$ or $Cu_{3+x}Sb_{1-x}Ti_xS_4$ can be designed (Figure 1). We report here on a new compound $Cu_{30}Ti_6Sb_2S_{32}$ (x = 0.75) which exhibits a novel ordered cubic $Cu_{30}Sb_2S_{32}$ sphalerite-like host lattice with features in between those of colusite $Cu_{26}Ti_2Sb_6S_{32}$ (x = 0.25) and Cu_4TiS_4 (x = 1). In this phase, the interstitial Ti^{4+} cations form tetrahedral-octahedral $[TiS_4]Cu_6$ complexes with surrounding copper atoms with unusually short Cu–Ti distances similar to the two other members. $Cu_{30}Ti_6Sb_2S_{32}$ is characterized by a semiconducting behavior and low thermal conductivity, whose mechanisms are investigated by combining experiments and theory in this study. Furthermore, we discussed the trends in the electronic bands and phonon dispersions for four members (Figure 1) of the Cu_3SbS_4–Cu_4TiS_4 system.

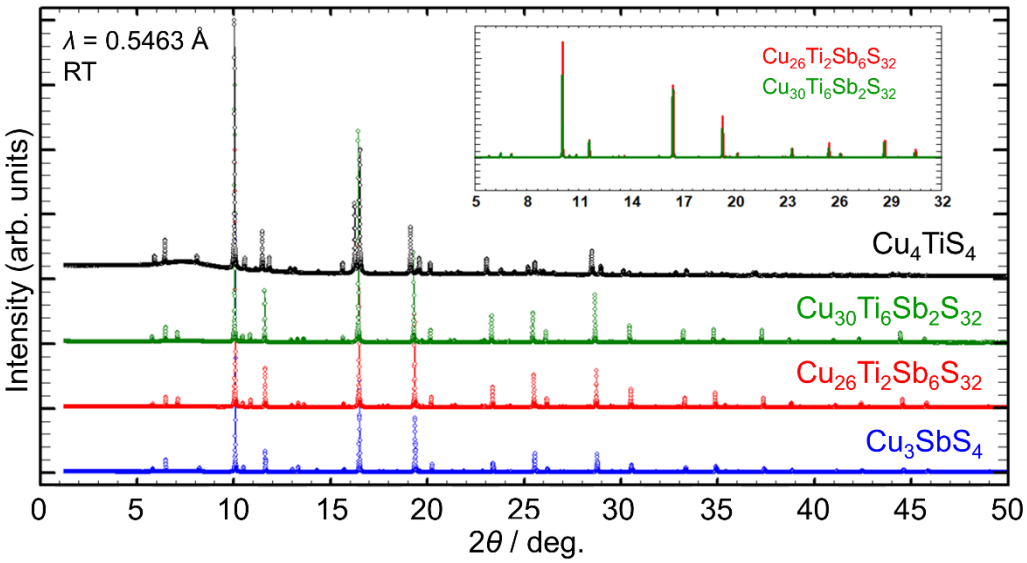

Figure 2. Synchrotron powder X-ray diffraction patterns of Cu_3SbS_4, $Cu_{26}Ti_2Sb_6S_{32}$, $Cu_{30}Ti_6Sb_2S_{32}$ and Cu_4TiS_4 recorded at room temperature (normalized data). The inset shows non-normalized data of $Cu_{26}Ti_2Sb_6S_{32}$ and $Cu_{30}Ti_6Sb_2S_{32}$.

RESULTS AND DISCUSSION

Room-temperature synchrotron powder X-ray diffraction (PXRD) patterns for the hot-pressed samples of the pseudo-binary system $(Cu_3SbS_4)_{1-x}(Cu_4TiS_4)_x$, *i.e.*, $Cu_{3+x}Sb_{1-x}Ti_xS_4$ with $x = 0$ (Cu_3SbS_4), $x = 0.25$ ($Cu_{26}Ti_2Sb_6S_{32}$), $x = 0.75$ ($Cu_{30}Ti_6Sb_2S_{32}$), and $x = 1$ (Cu_4TiS_4) are shown in Figure 2. A qualitative analysis of these measurements indicates that the diffraction pattern for the new compound $Cu_{30}Ti_6Sb_2S_{32}$ is very similar to that of colusite $Cu_{26}Ti_2Sb_6S_{32}$ (space group $P\bar{4}3n$). No peak splitting is observed in the patterns of $Cu_{30}Ti_6Sb_2S_{32}$ (Figure S1) and $Cu_{26}Ti_2Sb_6S_{32}$ (Figure S2), whereas a splitting is observed for Cu_3SbS_4 (Figure S3) and Cu_4TiS_4 (Figure S4) due to their tetragonal symmetry (space group $I\bar{4}2m$)[43,44] (*e.g.*, peaks at $2\theta \sim 16.5°$ are indexed to the (440) reflection in cubic structures and to the (220) and (204) reflections in tetragonal structures). Taking into account the absence of an inversion center as expected for a sphalerite derivative phase, the extinction rules for $Cu_{30}Ti_6Sb_2S_{32}$ agree with those for $Cu_{26}Ti_2Sb_6S_{32}$, indicating that this new compound crystallizes also in a cubic structure of space group $P\bar{4}3n$. The diffraction peaks for $Cu_{30}Ti_6Sb_2S_{32}$ are systematically shifted towards lower angles compared to colusite $Cu_{26}Ti_2Sb_6S_{32}$, indicating a slightly larger unit cell parameter for the former.

Considering that $Cu_{26}Ti_2Sb_6S_{32}$ ($x = 0.25$) and $Cu_{30}Ti_6Sb_2S_{32}$ ($x = 0.75$) are both members of the pseudo-binary system $Cu_{3+x}Sb_{1-x}Ti_xS_4$, a structural model was used for $Cu_{30}Ti_6Sb_2S_{32}$ ($x = 0.75$) based on the relationships between Cu_3SbS_4 ($x = 0$), $Cu_{26}Ti_2Sb_6S_{32}$ ($x = 0.25$), and Cu_4TiS_4 ($x = 1$).

Table 1. Crystal structure data of the Cu_3SbS_4 and Cu_4TiS_4 compounds from Rietveld analysis of the room-temperature synchrotron powder X-ray diffraction data.

Cu_3SbS_4 $I\bar{4}2m$				Cu_4TiS_4 $I\bar{4}2m$			
$R_{Bragg} = 2.44$, $R_F = 1.43$				$R_{Bragg} = 4.28$, $R_F = 3.32$			
$R_{wp} = 3.66$, $R_{exp} = 0.96$, $\chi^2 = 14.7$				$R_{wp} = 2.73$, $R_{exp} = 1.04$, $\chi^2 = 6.95$			
$a = 5.3876(1)$ Å, $c = 10.7509(1)$ Å				$a = 5.4642(1)$ Å, $c = 10.5889(1)$ Å			
Site	Atom	*x*, *y*, *z*	*B* / Å^2	Site	Atom	*x*, *y*, *z*	*B* / Å^2
2*a*	Sb	0, 0, 0	0.52(1)	2*a*	Ti	0, 0, 0	0.48(3)
2*b*	Cu	0, 0, 1/2	1.43(1)	2*b*	—	—	—
4*c*	—	—	—	4*c*	Cu	0, 1/2, 0	1.41(2)
4*d*	Cu	0, 1/2, 1/4	1.42(1)	4*d*	—	—	—
4*e*	—	—	—	4*e*	Cu	0, 0, 0.2602(1)	1.42(3)
8*i*	S	0.2542(1), x, 0.1291(1)	0.74(1)	8*i*	S	0.2418(2), x, 0.1254(2)	0.89(2)
Cu–S: 2.314 Å (average)				Cu–S: 2.344 Å (average)			
Sb–S: 2.383 Å				Ti–S: 2.292 Å			

Table 2. Crystal structure data of the $Cu_{26}Ti_2Sb_6S_{32}$ and $Cu_{30}Ti_6Sb_2S_{32}$ compounds from Rietveld analysis of the room-temperature synchrotron powder X-ray diffraction data.

$Cu_{26}Ti_2Sb_6S_{32}$ $P\bar{4}3n$				$Cu_{30}Ti_6Sb_2S_{32}$ $P\bar{4}3n$			
R_{Bragg} = 2.87 R_F = 4.98				R_{Bragg} = 5.62 R_F = 5.11			
R_{wp} = 4.09, R_{exp} = 0.97, χ^2 = 18.0				R_{wp} = 4.97, R_{exp} = 0.97, χ^2 = 26.5			
a = 10.7840(1) Å				*a* = 10.8084(1) Å			
Site	Atom	*x*, *y*, *z*	*B* / Å^2	Site	Atom	*x*, *y*, *z*	*B* / Å^2
2*a*	Ti	0, 0, 0	0.41(5)	2*a*	Sb	0, 0, 0	0.81(3)
6*b*	—	—	—	6*b*	Cu	0, 1/2, 1/2	1.13(3)
6*c*	Sb	1/4, 1/2, 0	0.58(1)	6*c*	Ti	1/4, 1/2, 0	0.24(3)
6*d*	Cu	1/4, 0, 1/2	1.52(2)	6*d*	—	—	—
8*e*	Cu	0.2477(2), *x*, *x*	1.33(2)	8*e*	—	—	—
12*f*	Cu	0.2558(1), 0, 0	1.22(2)	12*f*	—	—	—
24*i*	—	—	—	24*i*	Cu	0.2487(1), 0.2443(1), −0.0037(2)	1.25(1)
8*e*	S	0.1226(2), *x*, *x*	0.58(7)	8*e*	S	0.1268(3), *x*, *x*	0.88(9)
24*i*	S	0.3751(1), 0.3700(1), 0.1267(2)	0.80(3)	24*i*	S	0.3703(2), 0.3747(2), 0.1212(2)	0.61(3)
Cu–S: 2.326 Å (average)				Cu–S: 2.340 Å (average)			
Sb–S: 2.377 Å				Sb–S: 2.374 Å			
Ti–S: 2.290 Å				Ti–S: 2.289 Å			

Sphalerite, Cu_3SbS_4, Cu_4TiS_4 and $Cu_{26}Ti_2Sb_6S_{32}$ could be described as a face-centered cubic (FCC) sulfur network interpenetrated with a FCC cationic network shifted of a vector [1/4, 1/4, 1/4] or [–1/4, –1/4, –1/4]. The Wyckoff sites of space group $F\bar{4}3m$ are 4*c* for the sulphur and 4*a* or 4*b* for the cations (Figures 1, S5).

Cu_3SbS_4 and Cu_4TiS_4 are tetragonal superstructures of sphalerite with space group $I\bar{4}2m$ and unit cell parameters $a \sim a_s$ and $c \sim 2a_s$ (Figure 1, Table 1), where a_s represents the cell parameter of the cubic sphalerite structure. The S sublattice is the same in the two structures with atoms located on one 8*i* site, while the crystallographic sites occupied by d^{10} cations (corresponding to one half of the tetrahedral sites of this tetragonal structure) are different. In Cu_3SbS_4, Cu and Sb atoms occupy, in an ordered fashion the sites 2*a* (Sb), 2*b* (Cu), and 4*d* (Cu), derived of the sphalerite structure by the splitting of the 4*a* site (Figure 1, S5). In Cu_4TiS_4, Cu atoms occupy the 4*c* and 4*e* sites, derived of sphalerite structure by splitting of the 4*b* site (Figure 1, S5). Hence, d^{10} cations of Cu_3SbS_4 occupy the interstitial empty sites of Cu_4TiS_4, and vice versa. Finally, in Cu_4TiS_4, Ti atoms (d^0 cations) occupy the 2*a* site occupied by Sb atoms in Cu_3SbS_4.

$Cu_{26}Ti_2Sb_6S_{32}$ is a cubic superstructure of sphalerite with space group $P\bar{4}3n$ and unit cell parameter $a \sim 2a_s$ (Figure 1, Table 2).[38] In this cubic structure, d^{10} cations (Cu and Sb atoms) occupy in an ordered way one half of the tetrahedral sites of the cubic sulphur sublattice, *i.e.*, the sites 6*c* (Sb), 6*d* (Cu), 8*e* (Cu), and 12*f* (Cu), generated by the splitting of site 4*b* of sphalerite structure; d^0 cations (Ti atoms) are located in the 2*a* site, derived from the 4*a* site of sphalerite (Figure 1, S5).

Because $Cu_{26}Ti_2Sb_6S_{32}$ and $Cu_{30}Ti_6Sb_2S_{32}$ appear to be structurally related (similar PXRD patterns (Figure 2), same space group, and equivalent unit cell parameters), a structural model for the latter compound was based on the same cubic sulphur sublattice (*i.e.*, S atoms on sites 8*e* and 24*i*) derived from the sphalerite structure (Figure 1, Table 2). Furthermore, one can expect that, in $Cu_{30}Ti_6Sb_2S_{32}$, the Cu and Sb atoms (d^{10} cations) should also occupy, in an ordered way, one half of the tetrahedral sites. Consequently, Cu and Sb atoms can be distributed over the 6*c*, 6*d*, 8*e* and 12*f* sites as in $Cu_{26}Ti_2Sb_6S_{32}$ or over the 2*a*, 6*b*, and 24*i* sites similarly to Cu_3SbS_4 (Figure 1, Table 2). Considering the number of Cu and Sb atoms in $Cu_{30}Ti_6Sb_2S_{32}$, the second possibility was considered to construct an ordered superstructure sphalerite network, with Cu atoms located on the 6*b* and 24*i* sites and Sb atoms on the 2*a* site (Figure 1, Table 2). In the sphalerite derivative tetragonal Cu_3SbS_4 and Cu_4TiS_4 phases, the positions of Ti and Sb atoms are swapped and Ti atoms in $Cu_{30}Ti_6Sb_2S_{32}$ were considered to occupy the 6*c* site (*i.e.* site occupied by Sb in $Cu_{26}Ti_2Sb_6S_{32}$).

Finally, the as-constructed structural model of $Cu_{30}Ti_6Sb_2S_{32}$, including two Cu sites (6*b*, 24*i*), one Ti site (6*c*), one Sb site (2*a*), and two S sites (8*e*, 24*i*) (Figure 1), was confirmed by the high-quality Rietveld refinement of the synchrotron PXRD data. Crystallographic parameters obtained from Rietveld refinements of the PXRD patterns (Figures S1–S4) for $Cu_{30}Ti_6Sb_2S_{32}$ as well as Cu_3SbS_4, $Cu_{26}Ti_2Sb_6S_{32}$, and Cu_4TiS_4, are summarized in Tables 1 and 2. $Cu_{30}Ti_6Sb_2S_{32}$ and $Cu_{26}Ti_2Sb_6S_{32}$ (colusite) have different site sets of Cu and the swapped positions of Ti and Sb that we mentioned before, form inverse cationic subnetworks « Ti_6Sb_2 » and « Ti_2Sb_6 » respectively. Note that Cu_3SbS_4 and $Cu_{26}Ti_2Sb_6S_{32}$ are single-phase samples, while $Cu_{30}Ti_6Sb_2S_{32}$ and Cu_4TiS_4 samples contain traces of the hexagonal form of covellite CuS (< 2 wt.%).

Despite different symmetry (tetragonal/cubic), the sphalerite derivative crystal structures in the pseudo-binary system $Cu_{3+x}Sb_{1-x}Ti_xS_4$ phases are strongly related, as illustrated by the interatomic distances of Cu–S (2.31-2.34 Å),

Sb–S (2.37-2.38 Å), and Ti–S (2.29 Å) within the four compounds (Tables 1 and 2). Moreover, these phases highlight common chemical and structural characteristics, *i.e.* sphalerite networks formed by the sulphur anions and the d^{10} cations (Cu and Sb atoms) with d^0 cations (Ti atoms) at interstitial positions.

Of special importance is the formation of tetrahedral-octahedral $[TiS_4]Cu_6$ complexes, which are ordered in the three structures in dimensionally distinct sub-units: isolated in $Cu_{26}Ti_2Sb_6S_{32}$ (x = 0.25), arranged as rows of corner-sharing $[TiS_4]Cu_6$ complexes for $Cu_{30}Ti_6Sb_2S_{32}$ (x = 0.75), as layers of corner-sharing $[TiS_4]Cu_6$ complexes for Cu_4TiS_4 (x = 1). (Figure 3). Thus, the dimensional arrangement of the $[TiS_4]Cu_6$ units in the pseudo-binary system $Cu_{3+x}Sb_{1-x}Ti_xS_4$ phases evolves from 0D (x = 0.25), to 1D (x = 0.75), to 2D (x = 1). It could be noted that, to the best of our knowledge, $Cu_{30}Ti_6Sb_2S_{32}$ is the first copper-based sulphide characterized by a 1D $[TS_4]Cu_6$ units with T = d^0 cation (*i.e.*, Ti^{4+}), since in mooihoekite, $Cu_9Fe_9S_{16}$, T is a d^5 cation (*i.e.*, Fe^{3+}).[45] $Cu_{30}Ti_6Sb_2S_{32}$ is a new representative of the group C, according to the crystal-structure classification proposed by Lemoine *et al.*[1]

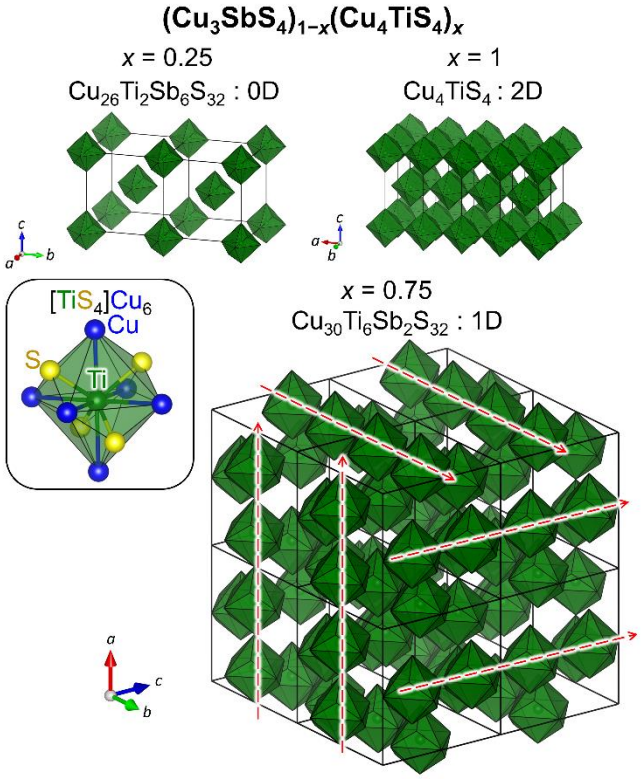

Figure 3. Representations of the tetrahedral-octahedral $[TiS_4]Cu_6$ complexes networks in the pseudo-binary system $(Cu_3SbS_4)_{1-x}(Cu_4TiS_4)_x$, *i.e.*, $Cu_{3+x}Sb_{1-x}Ti_xS_4$: $Cu_{26}Ti_2Sb_6S_{32}$ (x = 0.25), $Cu_{30}Ti_6Sb_2S_{32}$ (x = 0.75) and Cu_4TiS_4 (x = 1).

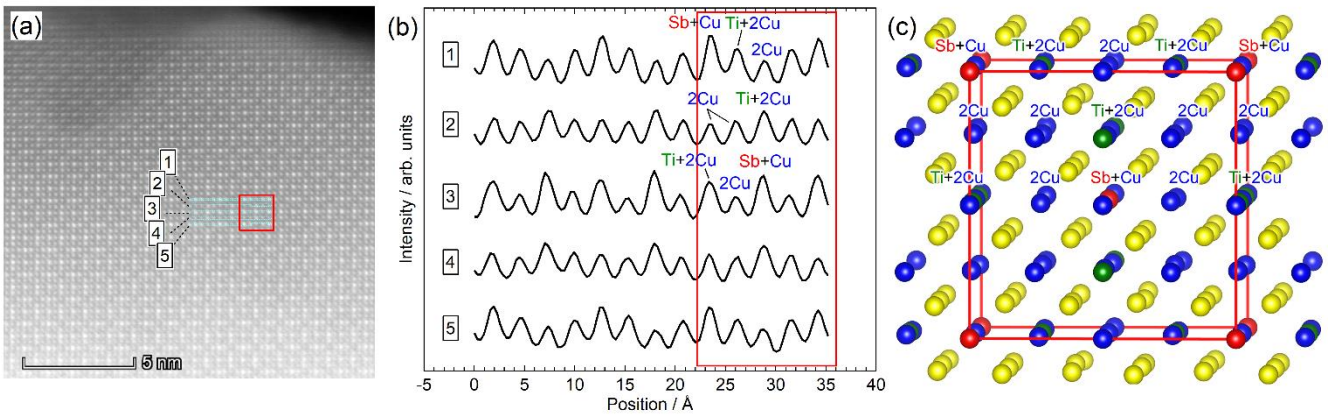

Figure 4. (a) Annular dark-field scanning transmission electron microscopy image of $Cu_{30}Ti_6Sb_2S_{32}$ along the four-fold axis. (b) Profiles of the intensities of the atomic columns for the lines denoted by 1–5 in (a). (c) The crystal structure of $Cu_{30}Ti_6Sb_2S_{32}$ along the four-fold axis. The labels of the atomic columns (e.g., Ti+2Cu) represents the number of atoms periodically contained in the columns. The atomic columns in (c) correspond to those surrounded by red square in (a) and (b).

The atomic configuration of the new compound $Cu_{30}Ti_6Sb_2S_{32}$ was also investigated by annular dark-field scanning transmission electron microscopy (ADF-STEM). As shown in Figure 4a, atomic columns (spots in the figure) along the four-fold axis are well aligned. The position and relative intensity of spots agree with those expected from the structure model described above (Figures 4b and 4c). More specifically, the Sb-rich columns (1 Sb + 1 Cu) exhibit the highest intensity; the Ti/Cu columns (1 Ti + 2 Cu) have higher intensity than Cu-only columns (2 Cu). The numeral (e.g., "2" for 2 Cu) denotes the number of atoms periodically contained in the columns (Figure 4c). The distance between Sb-rich columns is 11 Å, which agrees with the lattice parameter a ~ 10.8 Å (Table 2).

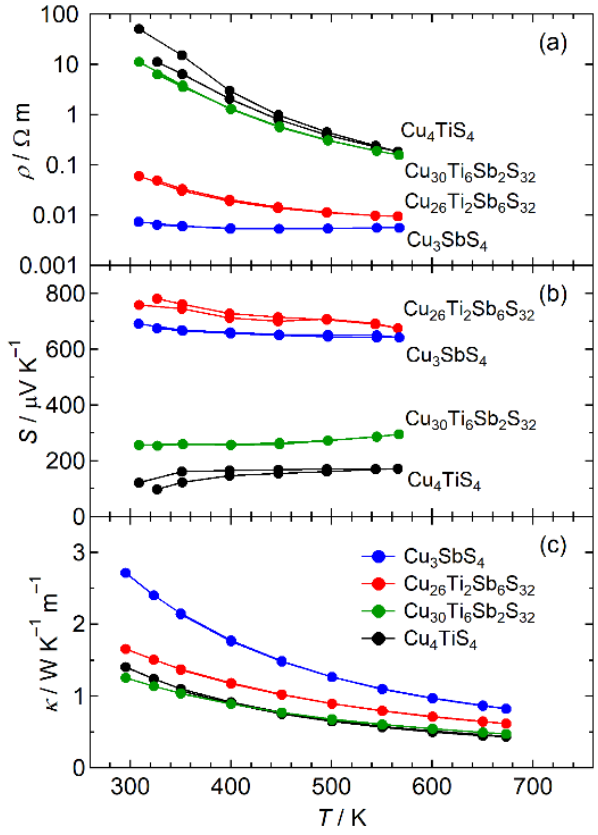

Figure 5. (a) Electrical resistivity, ρ, (b) Seebeck coefficient, S, and (c) thermal conductivity, κ, for the hot-pressed samples of Cu_3SbS_4, $Cu_{26}Ti_2Sb_6S_{32}$, $Cu_{30}Ti_6Sb_2S_{32}$ and Cu_4TiS_4.

The relative density of the hot-pressed samples evaluated from mass and dimensions was higher than 98–99 % of the theoretical density. Secondary electron images and backscattered electron images showed that samples are dense and homogeneous (Figure S6). Temperature dependence of electrical resistivity, ρ, and Seebeck coefficient, S, for the hot-pressed samples of the pseudo-binary system $Cu_{3+x}Sb_{1-x}Ti_xS_4$ with x = 0 (Cu_3SbS_4), x = 0.25 ($Cu_{26}Ti_2Sb_6S_{32}$), x = 0.75 ($Cu_{30}Ti_6Sb_2S_{32}$), and x = 1 (Cu_4TiS_4) are shown in Figure 5. Because the samples of Cu_3SbS_4 and $Cu_{26}Ti_2Sb_6S_{32}$ are known to partially decompose in a low-pressure atmosphere above 600 K,[14,38] the maximum temperature of the measurement was set at 565 K. The electrical resistivity, ρ, exhibits values in excess of 10^{-3} Ω m and semiconducting temperature dependence (Figure 5a). The positive sign of S indicates that hole carriers dominate the electronic conduction for all compounds (Figure 5b). $Cu_{30}Ti_6Sb_2S_{32}$ and Cu_4TiS_4 exhibit much higher ρ and significantly lower S values compared with Cu_3SbS_4 and $Cu_{26}Ti_2Sb_6S_{32}$. As a result, the power factors, $S^2\rho^{-1}$, of the former two compounds ($< 10^{-3}$ mWK^{-2}m^{-1}) are much smaller than that of the latter two compounds (10^{-2}–10^{-1} mWK^{-2}m^{-1}). For $Cu_{30}Ti_6Sb_2S_{32}$, we failed in obtaining reliable carrier concentration (Hall voltage) and carrier mobility because of the high electrical resistance of the sample. Therefore, it is difficult to discuss mechanisms of the combination of higher ρ and lower S.

Note that, unlike $Cu_{26}Ti_2Sb_6S_{32}$ colusite, we did not succeed in hole-carrier doping for the new compound $Cu_{30}Ti_6Sb_2S_{32}$ and as well for Cu_4TiS_4. This doping blockade phenomenon is likely related to the structural characteristics of these two compounds where all copper ions are involved in $[TiS_4]Cu_6$ complexes (Figure 3). We conjecture that hole carriers cannot be introduced on Cu cations which belong to the complexes due to the strong interactions between the interstitial T (here Ti) cation and the surrounding Cu cations. Consequently, the mixed valence Cu^+-Cu^{2+} required for hole delocalization on the Cu-S framework[42] is no more stable. The mechanism of doping blockade for $Cu_{30}Ti_6Sb_2S_{32}$ and Cu_4TiS_4 will be investigated in a future work for other copper sulphides, as it is a crucial constraint for the design of copper-based sulphides with dopable characteristics for thermoelectric applications.

Figure 6 shows electronic bands dispersion calculated for Cu_3SbS_4, $Cu_{26}Ti_2Sb_6S_{32}$,[38] $Cu_{30}Ti_6Sb_2S_{32}$, and Cu_4TiS_4. Cu_3SbS_4 and $Cu_{26}Ti_2Sb_6S_{32}$ have a direct theoretical band gap of E_g~0.4 eV (Figures 6a, 6b), while $Cu_{30}Ti_6Sb_2S_{32}/Cu_4TiS_4$ have indirect gaps of E_g~1.4/1.8 eV (Figures 6c, 6d). The top of the valence band manifold includes heavy and light bands with contributions from Cu and S orbitals for all compounds (Figure S7). While in Cu_3SbS_4 at the edge of the valence band, there are three valleys that are degenerate at Γ; the other compounds show a richer multivalley band structure. The dimensionality of the arrangement of tetrahedral-octahedral $[TiS_4]Cu_6$ complexes mentioned above does not change the (dimensionality of) band which seem to stay 3D. The complexity of the structure is such that the system, overall, doesn't modify its dimensionality.

For Sb-containing compounds, the lowest conduction band is mainly composed of Sb and S orbitals. The larger band gap for $Cu_{30}Ti_6Sb_2S_{32}$ compared with $Cu_{26}Ti_2Sb_6S_{32}$ results from the increase in the energy of conduction (Sb-S) band and its narrowed band width. The latter characteristic is probably caused by the more isolated nature of SbS_4 tetrahedra in $Cu_{30}Ti_6Sb_2S_{32}$ (Figure 1). For Cu_4TiS_4, the absence of Sb leads to the largest band gap in this series.

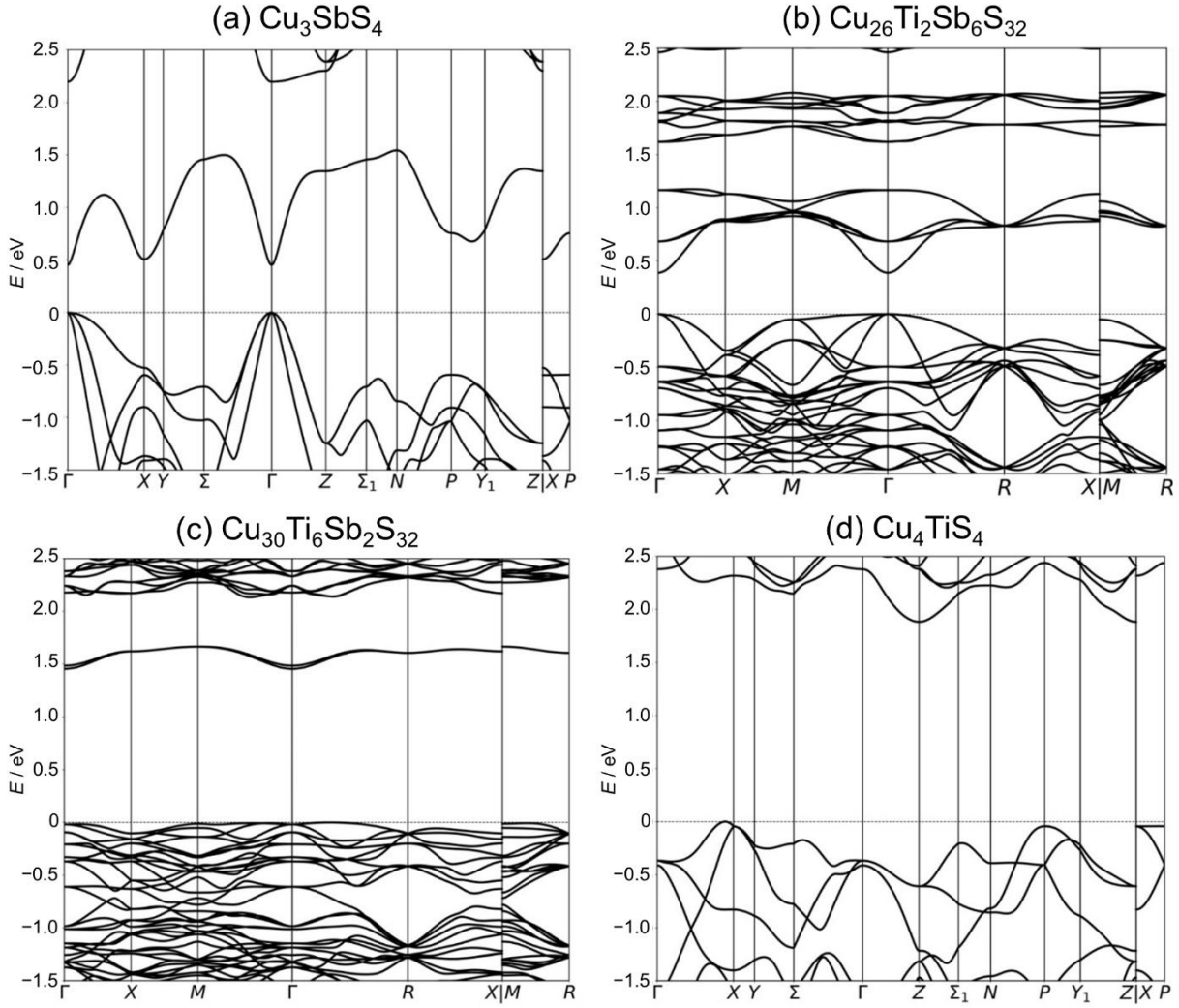

Figure 6. Electronic band dispersion for (a) Cu_3SbS_4, (b) $Cu_{26}Ti_2Sb_6S_{32}$, (c) $Cu_{30}Ti_6Sb_2S_{32}$, and (d) Cu_4TiS_4.

We examined the electronic structure experimentally by analyzing diffuse reflectance spectra (Figure S8). Figure 7 shows the plot for optical band gap determination. With reference to the calculation results, $(F(R_\infty)h\nu)^2$ or $(F(R_\infty)h\nu)^{1/2}$ are plotted for direct gap, *i.e.*, Cu_3SbS_4 and $Cu_{26}Ti_2Sb_6S_{32}$, or for indirect gap, *i.e.*, $Cu_{30}Ti_6Sb_2S_{32}$ and Cu_4TiS_4, as function of $h\nu$. The Kubelka-Munk function is indicated with $F(R_\infty)$ and $h\nu$ is the incident photon energy in eV. The linear part of $(F(R_\infty)h\nu)^2$ and $(F(R_\infty)h\nu)^{1/2}$ was extrapolated to a "baseline" (dotted line in Figure 7) and the energy of intersection was defined as E_g. For Cu_3SbS_4, E_g was estimated to be 0.9 eV (Figure 7a), which well agrees with a reported value,[46] but matches the computational results only qualitatively — the misalignment may be due to the limits of the theoretical calculation or can be justified by the fact that the Sb-derived energy levels at the bottom of the conduction band are distributed around 1.0 eV. For $Cu_{26}Ti_2Sb_6S_{32}$, $(F(R_\infty)h\nu)^2$ begin an upward trend at $h\nu$ = 0.9 eV in (Figure 7a), which can be attributed to the energy gap between the top of the valence band at Γ point and the isolated manifold around 0.9 eV (Figure 6). An additional increase in $(F(R_\infty)h\nu)^2$ (light absorption in the raw data) starting at $h\nu = 1.2$ eV indicating the existence of an additional energy gap that it is qualitatively reproduced in the band structure (above 1.2 eV). Other interpretation may be possible considering theoretical underestimation of the band gap. For $Cu_{30}Ti_6Sb_2S_{32}$ and Cu_4TiS_4, E_g was estimated to be 1.2/1.4 eV and 2.1 eV (indirect, Figures 7b), respectively. The values of E_g of Sb-containing systems are close to the value (1.4 eV) which gives the maximum theoretical efficiency of conversion from solar power to electrical power (Shockley-Queisser limit). Photoelectric conversion characteristics of the materials should be investigated.

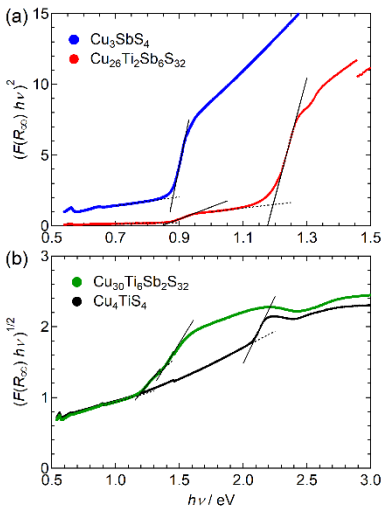

Figure 7. Transformed reflectance spectrum plots for the non-sintered samples of (a) Cu_3SbS_4, (a) $Cu_{26}Ti_2Sb_6S_{32}$, (b) $Cu_{30}Ti_6Sb_2S_{32}$ and (b) Cu_4TiS_4. Solid and dotted lines are fits to the data, the latter of which is used to consider the baseline for the estimation of optical band gap.

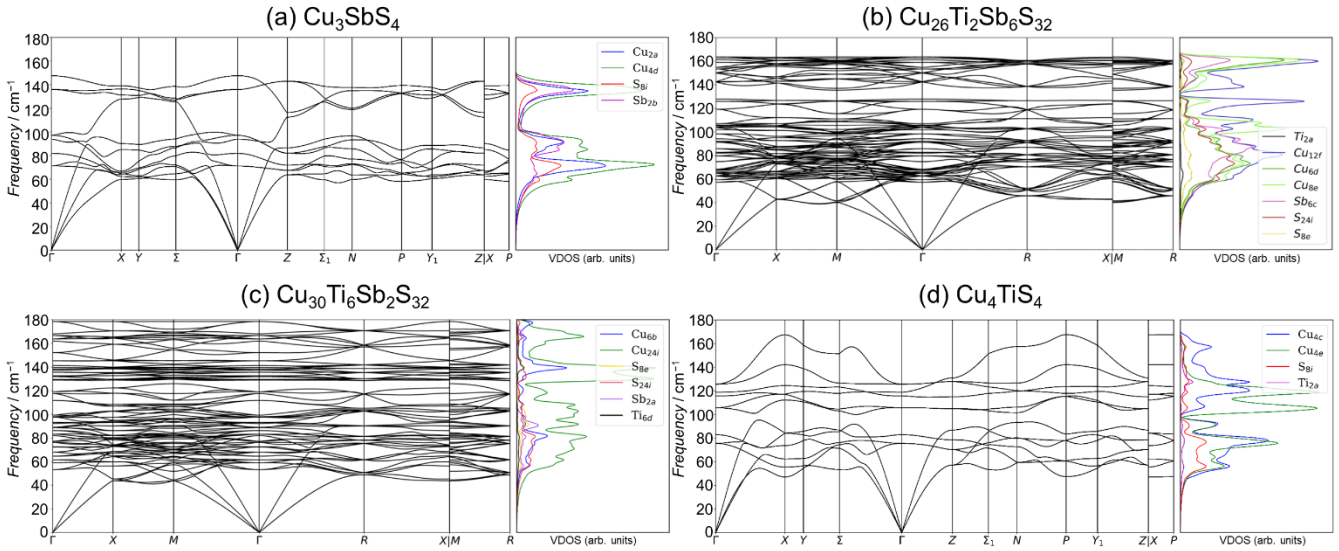

Figure 8. Phonon band dispersion and atom-projected density of states for (a) Cu_3SbS_4, (b) $Cu_{26}Ti_2Sb_6S_{32}$, (c) $Cu_{30}Ti_6Sb_2S_{32}$, and (d) Cu_4TiS_4.

Due to the semiconducting nature of our samples in the pseudo-binary system $Cu_{3+x}Sb_{1-x}Ti_xS_4$, thermal conductivity, κ, is governed by its lattice component. The κ values decrease with increasing temperature (Figure 5c), indicating that Umklapp processes are the dominant mechanism in phonon scattering for all compounds. The value of κ decreases from Cu_3SbS_4 (x = 0), to $Cu_{26}Ti_2Sb_6S_{32}$ (x = 0.25) to $Cu_{30}Ti_6Sb_2S_{32}$ (x = 0.75) and Cu_4TiS_4 (x = 1.0). The thermal conductivity of the new compound $Cu_{30}Ti_6Sb_2S_{32}$ is as low as 0.5 W K^{-1} m^{-1} (Figure 5c). The low κ for $Cu_{26}Ti_2Sb_6S_{32}$, $Cu_{30}Ti_6Sb_2S_{32}$, and Cu_4TiS_4 would be attributed to the small grain size (< 1 μm) in the sample (Figure S6) and their intrinsic properties partially reflected in the phonon dispersions (Figure 8). We underline the contribution of Cu dominated vibration at low frequency as observed in other copper sulphides. All compounds have optical modes lying below 180 cm^{-1}, which mainly involve the vibrations of Cu, Sb, and S. The dimensionality of the arrangement of tetrahedral-octahedral $[TiS_4]Cu_6$ complexes is probably secondary as well on the overall phonon dispersions. For all compounds except Cu_3SbS_4, optical modes exist at 40–60 cm^{-1}. This characteristic and the large number of optical modes are consistent with the low κ for $Cu_{26}Ti_2Sb_6S_{32}$ and $Cu_{30}Ti_6Sb_2S_{32}$. The phonon dispersion of Cu_3SbS_4 and Cu_4TiS_4 differ only slightly, the reduction in κ for Cu_4TiS_4 is due to effects beyond the phonon spectrum: anharmonicities and extrinsic scattering phenomena such as small grain size (Figure S6).

CONCLUSIONS

In summary, by using a pseudo-binary approach in the $(Cu_3SbS_4)_{1-x}(Cu_4TiS_4)_x$ system, we have discovered a compound, $Cu_{30}Ti_6Sb_2S_{32}$. The crystal structure of $Cu_{30}Ti_6Sb_2S_{32}$ (x = 0.75) is characterized by sphalerite-like network and interstitial Ti atoms, which is closely related to the structure of $Cu_{26}Ti_2Sb_6S_{32}$ colusite (x = 0.25) and combines the features of Cu_3SbS_4 (x = 0) and Cu_4TiS_4 (x = 1). Interestingly, the three structures of $Cu_{30}Ti_6Sb_2S_{32}$, $Cu_{26}Ti_2Sb_6S_{32}$, and Cu_4TiS_4 are distinguished by the dimensionality of the arrangement of tetrahedral-octahedral $[TiS_4]Cu_6$ complexes.

$Cu_{30}Ti_6Sb_2S_{32}$ and other three compounds exhibit semiconducting properties and low thermal conductivity. Combining experiments and theory, we demonstrate the nature of band gap and vibrational properties for low thermal conductivity. Based on this research, we propose crystal structure design using a pseudo-binary system to discover new materials. Our work in the ternary sphalerite derivative compounds with and without interstitial cations lead to the discovery of copper-based sulphide, $Cu_{30}Ti_6Sb_2S_{32}$. We expect this strategy to be successful also for selenides and tellurides providing a way to improve the efficiency of applications such as thermoelectric and photovoltaic devices.

EXPERIMENTAL AND COMPUTATIONAL DETAILS

We synthesized polycrystalline samples with compositions of $Cu_{3+x}Sb_{1-x}Ti_xS_4$ (x = 0, 0.25, 0.75, and 1). The elements—Cu (99.99%, wire), Ti (99.99%, powder), Sb (99.9999%, grain), S (99.99%, powder) from Kojundo Chemical Lab. Co., Ltd.—were weighed according to the target compositions for the x = 0.25, 0.75, and 1.0 samples. The elements were sealed in an evacuated quartz tube and heated to 1173 K (x = 0.25) or 1273 K (x = 0.75, 1) for 24 h. A slow heating rate of 100 Kh^{-1} was applied to avoid excessive sulfur vapor pressure inside the tube. For the x = 0 sample, starting with the stoichiometric composition led to the formation of a secondary phase, $Cu_{12}Sb_4S_{13}$. Therefore, we devised a two-step synthesis process to prepare phase-pure samples. The elements were weighed according to the composition $Cu_{12}Sb_4S_{13}$. The obtained sample was then pulverized using an agate mortar and the composition modified with the addition of sulfur powder according to the target concentrations (Cu_3SbS_4). The mixture was molded into a pellet, enclosed in an evacuated quartz tube, and then subjected to a heat treatment at 673 K for 50 h. The annealed samples of x = 0 as well as reacted (melted) samples of x = 0.25, 0.75, and 1.0 were pulverized using a planetary ball mill (PULVERISETTE 7 premium line, FRITSCH) operating at room temperature at a disk rotation speed of 450 rpm for 1 h. The sample powder (~3.5 g) was put into a jar (20 mL) together with seven balls of 10 mm diameter in an Ar atmosphere. The jar and balls were made of tungsten carbide (WC). Each pulverized sample was then loaded into a WC die with an inner diameter of 10 mm and sintered at 773 K for 20 min in a flowing N_2 atmosphere under a uniaxial pressure of 200 MPa in a hot-press sintering furnace (PLASMAN CSP-I-03121, S. S. Alloy). The sintered samples were cut and polished into bars (1.1–1.8 mm × 1.8–2.4 mm × 7.4–9.7 mm) and disks (10 mmϕ × 2 mm) to measure the thermoelectric properties. The hot-pressed samples were characterized by powder X-ray diffraction (PXRD), scanning electron microscopy (SEM, JCM-6000Plus NeoScope, JEOL), and annular dark-field scanning transmission electron microscopy (ADF-STEM).

PXRD data of samples arising from the pseudo-binary system $Cu_{3+x}Sb_{1-x}Ti_xS_4$ (x = 0, 0.25, 0.75, and 1), were collected at room temperature on the CRISTAL beamline at SOLEIL synchrotron (Saint-Aubin, France). The hot-pressed samples were finely ground, inserted into quartz capillaries of diameter 0.3 mm in order to avoid the necessity to correct the data for absorption, and sealed under vacuum. Acquisitions were performed at energy of 22.695 keV (λ = 0.5463 Å) using a two-circle diffractometer equipped with a Mythen detector bank composed of nine elements covering an angular range of ~50°.[47] Final diffraction patterns were obtained by the average of data acquired by the nine elements during a continuous scan of 60° counting 10 s for each step of 1°. The analysis of the diffraction patterns was performed by Rietveld refinement using the FullProf and WinPlotr software packages.[48,49] Background contribution was estimated manually. Zero-point shift, lattice parameters, peak shape parameters, asymmetry parameters, fractional atomic coordinates and isotropic displacement parameters (i.e. Debye–Waller factors B_{iso}) were systematically refined.

Atomic-resolution observations were performed on powdered sample of $Cu_{3+x}Sb_{1-x}Ti_xS_4$ with x = 0.75 ($Cu_{30}Ti_6Sb_2S_{32}$) using a transmission electron microscope (Titan Cubed 60-300 G2, Thermo Fisher Scientific), which is equipped with a spherical aberration corrector (DCOR, CEOS) for the probe-forming lens system. The microscope was operated in the STEM mode at an accelerating voltage of 300 kV. The convergence semiangle of the electron probe was set to 18 mrad. The typical probe diameter was less than 0.1 nm. An annular dark-field (ADF) detector was positioned to detect scattered electrons with an angular range from 38 to 184 mrad.

The electrical resistivity, ρ, and Seebeck coefficient, S, were simultaneously measured at T = 300–565 K in a low-pressure helium atmosphere using a measurement system (ZEM-3, ADVANCE RIKO). Thermal diffusivity, α, was measured at T = 300–673 K in a flowing Ar atmosphere using a light flash apparatus (LFA-467 HT HyperFlash®). These data were used to calculate $\kappa = \alpha C_{DP} d_s$, where C_{DP} is the Dulong–Petit value of specific heat and d_s is the bulk density. Diffuse reflectance spectra were recorded in the wavelength range of 220–2300 nm using a UV-VIS-NIR spectrophotometer (V-570, JASCO).

Band structure, density of states, and phonon dispersions were computed using the Quantum EXPRESSO package[50] as integrated in AFLOWπ[51] with PBEsol pseudopotentials (we used extended basis version of the PSLibrary[52] the for bands and the standard solid-state pseudopotentials library for the phonons[53] corrected with a ACBNo[54] Hubbard U (Table S1)). We chose an energy cutoff of 60 Ry, a 4 × 4 × 4 (shifted) integration grid. Electronic transport coefficients were evaluated with PAOFLOW[55]. Phonons were computed with the finite difference method using a 2 × 2 × 2 supercell.

ASSOCIATED CONTENT

Supporting Information. Rietveld refinements results of PXRD patterns, Crystal structure representations, SEM images, Atom-projected electron density of states, Diffuse reflectance spectra, Hubbard U correction computed with the ACBN0 approach.

This material is available free of charge via the Internet at http://pubs.acs.org.

ACKNOWLEDGMENT

K.S. is grateful to Dr. A. Nagaoka for fruitful discussion. This work was financially supported by JSPS KAKENHI (Grant no. JP20H02440 (K.S.)) and grants from the International Joint Research Program for Innovative Energy Technology funded by METI and Research and Development Program for Promoting Innovative Clean Energy Technologies through International Collaboration (Grant No. JPNP20005) funded by NEDO. E.G. and P.L. acknowledge the financial support of CNRS through the International Emerging Actions program (EXPRESS project). Crystal structures were visualized using software VESTA[56].

AUTHOR INFORMATION

Corresponding Authors

*Koichiro Suekuni − Department of Applied Science for Electronics and Materials, Interdisciplinary Graduate School of Engineering Sciences, Kyushu University, Kasuga, Fukuoka 816−8580, Japan; Transdisciplinary Research and Education Center for Green Technologies, Kyushu University, Kasuga, Fukuoka 816-8580, Japan; orcid.org/0000-0002-0515-4864; Email: suekuni.koichiro.063@m.kyushu-u.ac.jp

* Pierric Lemoine − Université de Rennes 1, CNRS, ISCR-UMR 6226, F-35000 Rennes, France; Institut Jean Lamour, UMR7198 CNRS, Université de Lorraine, 54011 Nancy, France; orcid.org/0000-0002-3465-7815; Email: pierric.lemoine@univ-lorraine.fr

*Emmanuel Guilmeau − CRISMAT, CNRS, Normandie Université, 14000 Caen, France; orcid.org/0000-0001-7439-088X; Email: emmanuel.guilmeau@ensicaen.fr

*Marco Fornari − Department of Physics and Science of Advanced Materials Program, Central Michigan University, Mt. Pleasant, Michigan 48859, United States; orcid.org/0000-0001-6527-8511; Email: forna1m@cmich.edu

Authors

Takashi Hagiwara – Department of Applied Science for Electronics and Materials, Interdisciplinary Graduate School of Engineering Sciences, Kyushu University, Kasuga, Fukuoka 816−8580, Japan

Carmelo Prestipino – Université de Rennes 1, CNRS, ISCR-UMR 6226, F-35000 Rennes, France
Erik Elkaim – Synchrotron Soleil, Saint-Aubin, BP 48, 91192 Gif-sur-Yvette, France; orcid.org/0000-0002-8541-7766

Andrew R. Supka – Department of Physics and Science of Advanced Materials Program, Central Michigan University, Mt. Pleasant, Michigan 48859, United States

Rabih Al Rahal Al Orabi – Department of Physics and Science of Advanced Materials Program, Central Michigan University, Mt. Pleasant, Michigan 48859, United State

Bernard Raveau – CRISMAT, CNRS, Normandie Université, 14000 Caen, France

Hikaru Saito – Institute for Materials Chemistry and Engineering, Kyushu University, Kasuga, Fukuoka 816-8580, Japan; orcid.org/0000-0001-9578-1433

Philipp Sauerschnig – Global Zero Emission Research Center, National Institute of Advanced Industrial Science and Technology (AIST), Tsukuba, Ibaraki 305-8569, Japan; orcid.org/0000-0003-4666-5262

Michihiro Ohta – Global Zero Emission Research Center, National Institute of Advanced Industrial Science and Technology (AIST), Tsukuba, Ibaraki 305-8569, Japan; orcid.org/0000-0002-9093-7117

Yui Kanemori – Department of Energy and Material Sciences, Faculty of Engineering Sciences, Kyushu University, Fukuoka 816-8580, Japan

Michitaka Ohtaki – Department of Applied Science for Electronics and Materials, Interdisciplinary Graduate School of Engineering Sciences, Kyushu University, Kasuga, Fukuoka 816−8580, Japan; Transdisciplinary Research and Education Center for Green Technologies, Kyushu University, Kasuga, Fukuoka 816-8580, Japan

Author Contributions

The manuscript was written through the contributions of all authors. All authors have given approval to the final version of the manuscript.

REFERENCES

(1) Lemoine, P.; Guélou, G.; Raveau, B.; Guilmeau, E. Crystal Structure Classification of Copper-based Sulphides as a Tool for the Design of Inorganic Functional Materials. *Angew. Chemie Int. Ed.* **2021**, anie.202108686. https://doi.org/10.1002/anie.202108686.

(2) Suekuni, K.; Tsuruta, K.; Ariga, T.; Koyano, M. Thermoelectric Properties of Mineral Tetrahedrites $Cu_{10}Tr_2Sb_4S_{13}$ with Low Thermal Conductivity. *Appl. Phys. Express* **2012**, *5* (5), 051201. https://doi.org/10.1143/APEX.5.051201.

(3) Lu, X.; Morelli, D. T.; Xia, Y.; Zhou, F.; Ozolins, V.; Chi, H.; Zhou, X.; Uher, C. High Performance Thermoelectricity in Earth-Abundant Compounds Based on Natural Mineral Tetrahedrites. *Adv. Energy Mater.* **2013**, *3* (3), 342–348. https://doi.org/10.1002/aenm.201200650.

(4) Suekuni, K.; Tsuruta, K.; Kunii, M.; Nishiate, H.; Nishibori, E.; Maki, S.; Ohta, M.; Yamamoto, A.; Koyano, M. High-Performance Thermoelectric Mineral $Cu_{12-x}Ni_xSb_4S_{13}$ Tetrahedrite. *J. Appl. Phys.* **2013**, *113* (4), 043712. https://doi.org/10.1063/1.4789389.

(5) Lu, X.; Morelli, D. T.; Xia, Y.; Ozolins, V. Increasing the Thermoelectric Figure of Merit of Tetrahedrites by Co-Doping with Nickel and Zinc. *Chem. Mater.* **2015**, *27* (2), 408–413. https://doi.org/10.1021/cm502570b.

(6) Barbier, T.; Lemoine, P.; Gascoin, S.; Lebedev, O. I.; Kaltzoglou, A.; Vaqueiro, P.; Powell, A. V.; Smith, R. I.; Guilmeau, E. Structural Stability of the Synthetic Thermoelectric Ternary and Nickel-Substituted Tetrahedrite Phases. *J. Alloys Compd.* **2015**, *634*, 253–262. https://doi.org/10.1016/j.jallcom.2015.02.045.

(7) Liu, M.-L.; Huang, F.-Q.; Chen, L.-D.; Chen, I.-W. A Wide-Band-Gap p-Type Thermoelectric Material Based on Quaternary Chalcogenides of Cu_2ZnSnQ_4 (*Q*=S,Se). *Appl. Phys. Lett.* **2009**, *94* (20), 202103. https://doi.org/10.1063/1.3130718.

(8) Zhang, R. zhi; Chen, K.; Du, B.; Reece, M. J. Screening for Cu-S Based Thermoelectric Materials Using Crystal Structure Features. *J. Mater. Chem. A* **2017**, *5* (10), 5013–5019. https://doi.org/10.1039/c6ta10607b.

(9) Bourgès, C.; Al Rahal Al Orabi, R.; Miyazaki, Y. Off-Stoichiometry Effect on Thermoelectric Properties of the New p-Type Sulfides Compounds Cu_2CoGeS_4. *J. Alloys Compd.*

2020, *826*, 154240. https://doi.org/10.1016/j.jallcom.2020.154240.

(10) Jiang, Q.; Yan, H.; Lin, Y.; Shen, Y.; Yang, J.; Reece, M. J. Colossal Thermoelectric Enhancement in $Cu_{2+x}Zn_{1-x}SnS_4$ Solid Solution by Local Disordering of Crystal Lattice and Multi-Scale Defect Engineering. *J. Mater. Chem. A* **2020**, *8* (21), 10909–10916. https://doi.org/10.1039/D0TA01595D.

(11) Nagaoka, A.; Yoshino, K.; Masuda, T.; Sparks, T. D.; Scarpulla, M. A.; Nishioka, K. Environmentally Friendly Thermoelectric Sulphide Cu_2ZnSnS_4 Single Crystals Achieving a 1.6 Dimensionless Figure of Merit *ZT*. *J. Mater. Chem. A* **2021**, *9* (28), 15595–15604. https://doi.org/10.1039/D1TA02978A.

(12) Chen, K.; Du, B.; Bonini, N.; Weber, C.; Yan, H.; Reece, M. J. Theory-Guided Synthesis of an Eco-Friendly and Low-Cost Copper Based Sulfide Thermoelectric Material. *J. Phys. Chem. C* **2016**, *120* (48), 27135–27140. https://doi.org/10.1021/acs.jpcc.6b09379.

(13) Chen, K.; Di Paola, C.; Du, B.; Zhang, R.; Laricchia, S.; Bonini, N.; Weber, C.; Abrahams, I.; Yan, H.; Reece, M. Enhanced Thermoelectric Performance of Sn-Doped Cu_3SbS_4. *J. Mater. Chem. C* **2018**, *6* (31), 8546–8552. https://doi.org/10.1039/c8tc02481b.

(14) Tanishita, T.; Suekuni, K.; Nishiate, H.; Lee, C. H.; Ohtaki, M. A Strategy for Boosting the Thermoelectric Performance of Famatinite Cu_3SbS_4. *Phys. Chem. Chem. Phys.* **2020**, *22* (4), 2081–2086. https://doi.org/10.1039/c9cp06233e.

(15) Tanimoto, T.; Suekuni, K.; Tanishita, T.; Usui, H.; Tadano, T.; Kamei, T.; Saito, H.; Nishiate, H.; Lee, C. H.; Kuroki, K.; Ohtaki, M. Enargite Cu_3PS_4 : A Cu–S-Based Thermoelectric Material with a Wurtzite-Derivative Structure. *Adv. Funct. Mater.* **2020**, *30* (22), 2000973. https://doi.org/10.1002/adfm.202000973.

(16) Shen, Y.; Li, C.; Huang, R.; Tian, R.; Ye, Y.; Pan, L.; Koumoto, K.; Zhang, R.; Wan, C.; Wang, Y. Eco-Friendly p-Type Cu_2SnS_3 Thermoelectric Material: Crystal Structure and Transport Properties. *Sci. Rep.* **2016**, *6* (1), 32501. https://doi.org/10.1038/srep32501.

(17) Guélou, G.; Pavan Kumar, V.; Carnevali, V.; Lebedev, O. I.; Raveau, B.; Couder, C.; Prestipino, C.; Lemoine, P.; Malaman, B.; Juraszek, J.; Candolfi, C.; Lenoir, B.; Al Rahal Al Orabi, R.; Fornari, M.; Guilmeau, E. Long-Range Cationic Order Collapse Triggered by S/Cl Mixed-Anion Occupancy Yields Enhanced Thermoelectric Properties in $Cu_5Sn_2S_7$. *Chem. Mater.* **2021**, *33* (23), 9425–9438. https://doi.org/10.1021/acs.chemmater.1c03434.

(18) Kumar, V. P.; Lemoine, P.; Carnevali, V.; Guélou, G.; Lebedev, O. I.; Raveau, B.; Al Rahal Al Orabi, R.; Fornari, M.; Candolfi, C.; Prestipino, C.; Menut, D.; Malaman, B.; Juraszek, J.; Suekuni, K.; Guilmeau, E. Local-Disorder-Induced Low Thermal Conductivity in Degenerate Semiconductor $Cu_{22}Sn_{10}S_{32}$. *Inorg. Chem.* **2021**, *60* (21), 16273–16285. https://doi.org/10.1021/acs.inorgchem.1c02105.

(19) Bourgès, C.; Lemoine, P.; Lebedev, O. I.; Daou, R.; Hardy, V.; Malaman, B.; Guilmeau, E. Low Thermal Conductivity in Ternary $Cu_4Sn_7S_{16}$ Compound. *Acta Mater.* **2015**, *97*, 180–190. https://doi.org/10.1016/j.actamat.2015.06.046.

(20) Pavan Kumar, V.; Paradis-Fortin, L.; Lemoine, P.; Le Caër, G.; Malaman, B.; Boullay, P.; Raveau, B.; Guélou, G.; Guilmeau, E. Crossover from Germanite to Renierite-Type Structures in $Cu_{22-x}Zn_xFe_8Ge_4S_{32}$ Thermoelectric Sulfides. *ACS Appl. Energy Mater.* **2019**, *2* (10), 7679–7689. https://doi.org/10.1021/acsaem.9b01681.

(21) Pavan Kumar, V.; Barbier, T.; Caignaert, V.; Raveau, B.; Daou, R.; Malaman, B.; Caër, G. Le; Lemoine, P.; Guilmeau, E. Copper Hyper-Stoichiometry: The Key for the Optimization of Thermoelectric Properties in Stannoidite $Cu_{8+x}Fe_{3-x}Sn_2S_{12}$. *J. Phys. Chem. C* **2017**, *121* (30), 16454–16461. https://doi.org/10.1021/acs.jpcc.7b02068.

(22) Pavan Kumar, V.; Paradis-Fortin, L.; Lemoine, P.; Caignaert, V.; Raveau, B.; Malaman, B.; Le Caër, G.; Cordier, S.; Guilmeau, E. Designing a Thermoelectric Copper-Rich Sulfide from a Natural Mineral: Synthetic Germanite $Cu_{22}Fe_8Ge_4S_{32}$. *Inorg. Chem.* **2017**, *56* (21), 13376–13381. https://doi.org/10.1021/acs.inorgchem.7b02128.

(23) Paradis-Fortin, L.; Guélou, G.; Pavan Kumar, V.; Lemoine, P.; Prestipino, C.; Merdrignac-Conanec, O.; Durand, G. R.; Cordier, S.; Lebedev, O. I.; Guilmeau, E. Structure, Microstructure and Thermoelectric Properties of Germanite-Type $Cu_{22}Fe_8Ge_4S_{32}$ Compounds. *J. Alloys Compd.* **2020**, *831*, 154767. https://doi.org/10.1016/j.jallcom.2020.154767.

(24) Tsujii, N.; Mori, T. High Thermoelectric Power Factor in a Carrier-Doped Magnetic Semiconductor $CuFeS_2$. *Appl. Phys. Express* **2013**, *6* (4), 043001. https://doi.org/10.7567/APEX.6.043001.

(25) Xie, H.; Su, X.; Zheng, G.; Yan, Y.; Liu, W.; Tang, H.; Kanatzidis, M. G.; Uher, C.; Tang, X. Nonmagnetic In Substituted $CuFe_{1-x}In_xS_2$ Solid Solution Thermoelectric. *J. Phys. Chem. C* **2016**, *120* (49), 27895–27902. https://doi.org/10.1021/acs.jpcc.6b10308.

(26) Qiu, P.; Zhang, T.; Qiu, Y.; Shi, X.; Chen, L. Sulfide Bornite Thermoelectric Material: A Natural Mineral with Ultralow Thermal Conductivity. *Energy Environ. Sci.* **2014**, *7* (12), 4000–4006. https://doi.org/10.1039/C4EE02428A.

(27) Guélou, G.; Powell, A. V.; Vaqueiro, P. Ball Milling as an Effective Route for the Preparation of Doped Bornite: Synthesis, Stability and Thermoelectric Properties. *J. Mater. Chem. C* **2015**, *3* (40), 10624–10629. https://doi.org/10.1039/C5TC01704A.

(28) Suekuni, K.; Kim, F. S.; Takabatake, T. Tunable Electronic Properties and Low Thermal Conductivity in Synthetic Colusites $Cu_{26-x}Zn_xV_2M_6S_{32}$ ($x \leq 4$, M = Ge, Sn). *J. Appl. Phys.* **2014**, *116* (6), 063706. https://doi.org/10.1063/1.4892593.

(29) Suekuni, K.; Kim, F. S.; Nishiate, H.; Ohta, M.; Tanaka, H. I.; Takabatake, T. High-Performance Thermoelectric Minerals: Colusites $Cu_{26}V_2M_6S_{32}$ (M = Ge, Sn). *Appl. Phys. Lett.* **2014**, *105* (13), 132107. https://doi.org/10.1063/1.4896998.

(30) Kikuchi, Y.; Bouyrie, Y.; Ohta, M.; Suekuni, K.; Aihara, M.; Takabatake, T. Vanadium-Free Colusites $Cu_{26}A_2Sn_6S_{32}$ (A = Nb, Ta) for Environmentally Friendly Thermoelectrics. *J. Mater. Chem. A* **2016**, *4* (39), 15207–15214. https://doi.org/10.1039/c6ta05945g.

(31) Kim, F. S.; Suekuni, K.; Nishiate, H.; Ohta, M.; Tanaka, H. I.; Takabatake, T. Tuning the Charge Carrier Density in the Thermoelectric Colusite. *J. Appl. Phys.* **2016**, *119* (17), 175105. https://doi.org/10.1063/1.4948475.

(32) Bouyrie, Y.; Ohta, M.; Suekuni, K.; Kikuchi, Y.; Jood, P.; Yamamoto, A.; Takabatake, T. Enhancement in the Thermoelectric Performance of Colusites $Cu_{26}A_2E_6S_{32}$ (A = Nb, Ta; E = Sn, Ge) Using E-Site Non-Stoichiometry. *J. Mater. Chem. C* **2017**, *5* (17), 4174–4184. https://doi.org/10.1039/c7tc00762k.

(33) Bourgès, C.; Bouyrie, Y.; Supka, A. R.; Al Rahal Al Orabi, R.; Lemoine, P.; Lebedev, O. I.; Ohta, M.; Suekuni, K.; Nassif, V.; Hardy, V.; Daou, R.; Miyazaki, Y.; Fornari, M.; Guilmeau, E. High-Performance Thermoelectric Bulk Colusite by Process Controlled Structural Disordering. *J. Am. Chem. Soc.* **2018**, *140* (6), 2186–2195. https://doi.org/10.1021/jacs.7b11224.

(34) Suekuni, K.; Shimizu, Y.; Nishibori, E.; Kasai, H.; Saito, H.; Yoshimoto, D.; Hashikuni, K.; Bouyrie, Y.; Chetty, R.; Ohta, M.; Guilmeau, E.; Takabatake, T.; Watanabe, K.; Ohtaki, M. Atomic-Scale Phonon Scatterers in Thermoelectric Colusites with a Tetrahedral Framework Structure. *J. Mater. Chem. A* **2019**, *7* (1), 228–235. https://doi.org/10.1039/c8ta08248k.

(35) Pavan Kumar, V.; Supka, A. R.; Lemoine, P.; Lebedev, O. I.; Raveau, B.; Suekuni, K.; Nassif, V.; Al Rahal Al Orabi, R.; Fornari, M.; Guilmeau, E. High Power Factors of Thermoelectric Colusites $Cu_{26}T_2Ge_6S_{32}$ (T = Cr, Mo, W): Toward Functionalization of the Conductive "Cu–S" Network. *Adv. Energy Mater.* **2019**, *9* (6), 1803249. https://doi.org/10.1002/aenm.201803249.

(36) Pavan Kumar, V.; Guélou, G.; Lemoine, P.; Raveau, B.; Supka, A. R.; Al Rahal Al Orabi, R.; Fornari, M.; Suekuni, K.; Guilmeau, E. Copper-Rich Thermoelectric Sulfides: Size-Mismatch Effect and Chemical Disorder in the $[TS_4]Cu_6$ Complexes of $Cu_{26}T_2Ge_6S_{32}$ (T=Cr, Mo, W) Colusites. *Angew. Chemie - Int. Ed.* **2019**, *58* (43), 15455–15463. https://doi.org/10.1002/anie.201908579.

(37) Guélou, G.; Pavan Kumar, V.; Bourhim, A.; Lemoine, P.; Raveau, B.; Supka, A.; Lebedev, O. I.; Al Rahal Al Orabi, R.;

Fornari, M.; Suekuni, K.; Guilmeau, E. Toppling the Transport Properties with Cationic Overstoichiometry in Thermoelectric Colusite: $[Cu_{26}Cr_2Ge_6]_{1+\delta}S_{32}$. *ACS Appl. Energy Mater.* **2020**, *3* (5), 4180–4185. https://doi.org/10.1021/acsaem.0c00726.

(38) Hagiwara, T.; Suekuni, K.; Lemoine, P.; Supka, A. R.; Chetty, R.; Guilmeau, E.; Raveau, B.; Fornari, M.; Ohta, M.; Al Rahal Al Orabi, R.; Saito, H.; Hashikuni, K.; Ohtaki, M. Key Role of d^0 and d^{10} Cations for the Design of Semiconducting Colusites: Large Thermoelectric *ZT* in $Cu_{26}Ti_2Sb_6S_{32}$ Compounds. *Chem. Mater.* **2021**, *33* (9), 3449–3456. https://doi.org/10.1021/acs.chemmater.1c00872.

(39) Shimizu, Y.; Suekuni, K.; Saito, H.; Lemoine, P.; Guilmeau, E.; Raveau, B.; Chetty, R.; Ohta, M.; Takabatake, T.; Ohtaki, M. Synergistic Effect of Chemical Substitution and Insertion on the Thermoelectric Performance of $Cu_{26}V_2Ge_6S_{32}$ Colusite. *Inorg. Chem.* **2021**, *60* (15), 11364–11373. https://doi.org/10.1021/acs.inorgchem.1c01321.

(40) Green, M. A.; Dunlop, E. D.; Hohl-Ebinger, J.; Yoshita, M.; Kopidakis, N.; Ho-Baillie, A. W. Y. Solar Cell Efficiency Tables (Version 55). *Prog. Photovoltaics Res. Appl.* **2020**, *28* (1), 3–15. https://doi.org/https://doi.org/10.1002/pip.3228.

(41) Hiroi, H.; Iwata, Y.; Adachi, S.; Sugimoto, H.; Yamada, A. New World-Record Efficiency for Pure-Sulfide Cu(In,Ga)S2 Thin-Film Solar Cell With Cd-Free Buffer Layer via KCN-Free Process. *IEEE J. Photovoltaics* **2016**, *6* (3), 760–763. https://doi.org/10.1109/JPHOTOV.2016.2537540.

(42) Raveau, B. Copper Mixed Valence Concept: "Cu(I)–Cu(II)" in Thermoelectric Copper Sulfides—an Alternative to "Cu(II)–Cu(III)" in Superconducting Cuprates. *J. Supercond. Nov. Magn.* **2020**, *33* (1), 259–263. https://doi.org/10.1007/s10948-019-05354-8.

(43) Klepp, K. O.; Gurtner, D. Synthesis and Crystal Structure of Cu_4TiS_4: A Novel Chalcogenide with Tetrahedrally Coordinated Titanium. *J. Alloys Compd.* **1996**, *243* (1–2), 19–22. https://doi.org/10.1016/S0925-8388(96)02363-8.

(44) Garin, J.; Parthé, E. The Crystal Structure of Cu_3PSe_4 and Other Ternary Normal Tetrahedral Structure Compounds with Composition 1_356_4. *Acta Crystallogr. Sect. B Struct. Crystallogr. Cryst. Chem.* **1972**, *28* (12), 3672–3674. https://doi.org/10.1107/s0567740872008568.

(45) Hall, S. R.; Rowland, J. F. The Crystal Structure of Synthetic Mooihoekite $Cu_9Fe_9S_{16}$. *Acta Crystallogr. Sect. B Struct. Crystallogr. Cryst. Chem.* **1973**, *29* (11), 2365–2372. https://doi.org/10.1107/S0567740873006710.

(46) Goto, Y.; Sakai, Y.; Kamihara, Y.; Matoba, M. Effect of Sn-Substitution on Thermoelectric Properties of Copper-Based Sulfide, Famatinite Cu_3SbS_4. *J. Phys. Soc. Japan* **2015**, *84* (4), 044706. https://doi.org/10.7566/JPSJ.84.044706.

(47) Schmitt, B.; Brönnimann, C.; Eikenberry, E. .; Gozzo, F.; Hörmann, C.; Horisberger, R.; Patterson, B. Mythen Detector System. *Nucl. Instruments Methods Phys. Res. Sect. A Accel. Spectrometers, Detect. Assoc. Equip.* **2003**, *501* (1), 267–272. https://doi.org/10.1016/S0168-9002(02)02045-4.

(48) Rodríguez-Carvajal, J. Recent Advances in Magnetic Structure Determination by Neutron Powder Diffraction. *Phys. B Condens. Matter* **1993**, *192* (1–2), 55–69. https://doi.org/10.1016/0921-4526(93)90108-I.

(49) Roisnel, T.; Rodríguez-Carvajal, J. WinPLOTR: A Windows Tool for Powder Diffraction Pattern Analysis. *Mater. Sci. Forum* **2001**, *378–381* (I), 118–123. https://doi.org/10.4028/www.scientific.net/msf.378-381.118.

(50) Giannozzi, P.; Baroni, S.; Bonini, N.; Calandra, M.; Car, R.; Cavazzoni, C.; Ceresoli, D.; Chiarotti, G. L.; Cococcioni, M.; Dabo, I.; Dal Corso, A.; de Gironcoli, S.; Fabris, S.; Fratesi, G.; Gebauer, R.; Gerstmann, U.; Gougoussis, C.; Kokalj, A.; Lazzeri, M.; Martin-Samos, L.; Marzari, N.; Mauri, F.; Mazzarello, R.; Paolini, S.; Pasquarello, A.; Paulatto, L.; Sbraccia, C.; Scandolo, S.; Sclauzero, G.; Seitsonen, A. P.; Smogunov, A.; Umari, P.; Wentzcovitch, R. M. QUANTUM ESPRESSO: A Modular and Open-Source Software Project for Quantum Simulations of Materials. *J. Phys. Condens. Matter* **2009**, *21* (39), 395502. https://doi.org/10.1088/0953-8984/21/39/395502.

(51) Supka, A. R.; Lyons, T. E.; Liyanage, L.; D'Amico, P.; Al Rahal Al Orabi, R.; Mahatara, S.; Gopal, P.; Toher, C.; Ceresoli, D.; Calzolari, A.; Curtarolo, S.; Nardelli, M. B.; Fornari, M. AFLOWπ: A Minimalist Approach to High-Throughput Ab Initio Calculations Including the Generation of Tight-Binding Hamiltonians. *Comput. Mater. Sci.* **2017**, *136*, 76–84. https://doi.org/10.1016/j.commatsci.2017.03.055.

(52) PSLibrary. https://dalcorso.github.io/pslibrary/ (date of access: July 10th)

(53) A standard solid-state pseudopotentials (SSSP) library optimized for precision or efficiency. https://www.materialscloud.org/discover/sssp/table/efficiency (date of access: July 10th)

(54) Agapito, L. A.; Curtarolo, S.; Buongiorno Nardelli, M. Reformulation of DFT+*U* as a Pseudohybrid Hubbard Density Functional for Accelerated Materials Discovery. *Phys. Rev. X* **2015**, *5* (1), 011006. https://doi.org/10.1103/PhysRevX.5.011006.

(55) Buongiorno Nardelli, M.; Cerasoli, F. T.; Costa, M.; Curtarolo, S.; De Gennaro, R.; Fornari, M.; Liyanage, L.; Supka, A. R.; Wang, H. PAOFLOW: A Utility to Construct and Operate on Ab Initio Hamiltonians from the Projections of Electronic Wavefunctions on Atomic Orbital Bases, Including Characterization of Topological Materials. *Comput. Mater. Sci.* **2018**, *143*, 462–472. https://doi.org/10.1016/j.commatsci.2017.11.034.

(56) Momma, K.; Izumi, F. VESTA 3 for Three-Dimensional Visualization of Crystal, Volumetric and Morphology Data. *J. Appl. Crystallogr.* **2011**, *44* (6), 1272–1276. https://doi.org/10.1107/S0021889811038970.

TOC figure

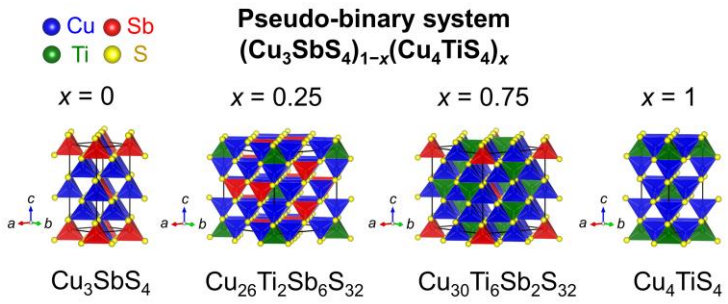
Cu
Sb
Ti
S
Pseudo-binary system
$(Cu_3SbS_4)_{1-x}(Cu_4TiS_4)_x$
x = 0
x = 0.25
x = 0.75
x = 1
c
a
b
Cu_3SbS_4
$Cu_{26}Ti_2Sb_6S_{32}$
$Cu_{30}Ti_6Sb_2S_{32}$
Cu_4TiS_4